

Tracking the distance to criticality in systems with unknown noise

Brendan Harris

School of Physics, The University of Sydney, NSW 2006, Australia

Leonardo L. Gollo

*The Turner Institute for Brain and Mental Health, School of Psychological Sciences,
and Monash Biomedical Imaging, Monash University, Victoria 3168, Australia*

Ben D. Fulcher

School of Physics, The University of Sydney, NSW 2006, Australia

(Dated: October 25, 2023)

Many real-world systems undergo abrupt changes in dynamics as they move across critical points, often with dramatic and irreversible consequences. Much of the existing theory on identifying the time-series signatures of nearby critical points—such as increased signal variance and slower timescales—is derived from analytically tractable systems, typically considering the case of fixed, low-amplitude noise. However, real-world systems are often corrupted by unknown levels of noise which can obscure these temporal signatures. Here we aimed to develop noise-robust indicators of the distance to criticality (DTC) for systems affected by dynamical noise in two cases: when the noise amplitude is either fixed, or is unknown and variable across recordings. We present a highly comparative approach to tackling this problem that compares the ability of over 7000 candidate time-series features to track the DTC in the vicinity of a supercritical Hopf bifurcation. Our method recapitulates existing theory in the fixed-noise case, highlighting conventional time-series features that accurately track the DTC. But in the variable-noise setting, where these conventional indicators perform poorly, we highlight new types of high-performing time-series features and show that their success is underpinned by an ability to capture the shape of the invariant density (which depends on both the DTC and the noise amplitude) relative to the spread of fast fluctuations (which depends on the noise amplitude). We introduce a new high-performing time-series statistic, termed the Rescaled Auto-Density (RAD), that distills these two algorithmic components. Our results demonstrate that large-scale algorithmic comparison can yield theoretical insights and motivate new algorithms for solving important practical problems.

I. INTRODUCTION

A critical point, or bifurcation point, marks the value of some control parameter at which the dynamical properties of a system undergo a qualitative change, such as the appearance or disappearance of an attractor [1]. Many phase transitions occur at critical points described by bifurcations in mathematical models of a system [2]. In spin glasses, a net magnetization emerges at a critical value of the temperature order parameter [3], while in cosmology, the temperature controls the electroweak phase transition and baryon (matter–antimatter) asymmetry [4]. The dynamics of complex systems—from the brain to biological swarms—can also be understood in terms of their vicinity to a critical point, with near-critical systems possessing a range of functional advantages [5]. In the brain, for example, traversing critical points is thought to mediate changes in behavioral and cognitive functions such as memory storage and retrieval, as well as visual attention and processing [6–9].

Crossing a critical point can have dangerous consequences. For example, generator voltages in power distribution networks undergo bifurcation and transition from fixed-point stability to unsafe oscillation at a critical value of system load [10, 11]. At so-called tipping points, where crossing a critical point leads to instability, the system may also change catastrophically as it

rapidly transitions to a new state [12, 13]. Catastrophes occur in simple physical systems, such as slipping events in wires under stress [14], as well as in models of sleep–wake transitions [15, 16], transitions to epileptic brain states [17, 18], and major climate events such as the desertification of North Africa [19]. Moreover, critical phenomena are studied across scientific domains, including physics [20, 21], neuroscience [5, 7], medicine [22, 23], biology [24], and engineering [25]. The ubiquity of critical phenomena calls for a noise-robust method that can predict how close a system is to a critical point [26]: to give warning of epileptic seizure [17, 18], anticipate power distribution failures [27], forecast imminent climate catastrophes [28], or to better control cognitive changes using brain stimulation [29].

Despite the ubiquity and diversity of critical systems, critical phenomena are remarkably linked by a common mathematical foundation: normal forms and bifurcation theory [12, 13]. This theory categorizes most systems near a critical point into a well-studied, analytical taxonomy of bifurcations [1, 30]. Moreover, a surprising number of systems exhibit relatively simple, codimension-one bifurcations [1, 31], including saddle-node bifurcations found in the dynamics of neuronal spiking [32], pitchfork bifurcations in Bose–Einstein condensates [33], or Hopf bifurcations in laser cavities [34], financial markets [35], the auditory system [36], thalamocortical models [37],

and models of interacting brain regions [38]. Each type of bifurcation is associated with a normal form—a dynamical equation that encapsulates the essential qualitative behavior near the critical point, regardless of the system [39]. With the allure of solving a plethora of real-world challenges simultaneously, much recent work has studied this unifying mathematical structure of critical phenomena with the aim of identifying universal indicators of criticality. For normal forms, and other systems that can be modeled analytically, this task is equivalent to estimating the control parameter that determines how close the system is to the bifurcation point. As such, a primary goal of studying normal forms has been to derive simple dynamical properties that diagnose how close any critical system is to a bifurcation point, a quantity which we term the *distance to criticality* (DTC) in this work.

Studies of normal forms and real-world critical systems have identified basic but universal dynamical characteristics that are informative of the DTC [40]: near a critical point, dynamics are more variable and evolve on a slower timescale [24, 41, 42]. Both properties can be understood as a byproduct of the flattening of the potential function of a system near the critical point. A flatter potential about a local minimum (fixed point) increases the return time when a system is perturbed [43] and slows the timescale of fluctuations in a system driven by noise; a phenomenon known as *critical slowing down* [41]. Because a flatter potential function also decreases the confinement of noise-related diffusion, the domain explored by a stochastic system will expand when the system is close to the critical point. Hence, the standard deviation of a time series increases near a bifurcation point, and has been shown to scale like a negative power of the control parameter when the strength of additive noise is close to zero [12, 44, 45]. Although properties of the potential naturally motivate standard deviation and autocorrelation as indicators of criticality, many related features are used to estimate the DTC in a variety of fields [40, 46], including: time-series skewness of chlorophyll in lake ecosystems [47]; increases in low-frequency fluctuations of voltage in electrical power systems [25]; spatial autocorrelation of coupled dynamical systems [48]; and other multivariate critical indicators [18, 49, 50].

In deriving statistical indicators for the vicinity of a system to a critical point, mathematical analyses typically assume the presence of a weak stochastic component relative to dominant deterministic dynamics [51]. Stochastic influences are typically classified as either: *measurement noise*, which is applied to the final signal independently from the underlying dynamics of the system; or *dynamical noise*, which is incorporated into the equations of motion and constantly perturbs the deterministic dynamics [52, 53]. Progress has been made in deriving scaling laws for critical indicators when the strength of dynamical noise is close to zero, such as the relationship between variance and the control parameter when approaching various bifurcations [12, 13]. Unfortunately, even noise with a small but non-vanishing strength com-

plicates the task of defining (let alone predicting) bifurcation points in stochastic systems [54, 55]. One common approach, which we operate under in this work, is to designate the bifurcation point as the value of the control parameter that divides invariant densities with distinct qualitative properties (see Sec. III C). For example, if dynamical noise is incorporated into the normal form of a pitchfork bifurcation, then the distribution of states visited by the system converges over time, for a fixed control parameter. The transition between a unimodal and bimodal invariant density, corresponding to appearance of a second attractor, occurs at the same value of the control parameter as bifurcation in the deterministic terms alone [56]. This splitting of the invariant density (see Sec. III C), termed a *phenomenological* bifurcation [51], tends to precede other types of bifurcation points defined by changes in dynamical measures (known as *dynamical* bifurcations) [56], and gives a natural definition for the critical point that we use here.

Many physical systems, however, are subject to noise that is not small relative to the scale of their deterministic dynamics. Moderate noise has been incorporated into models of critical transitions to neuron spiking [32], climate tipping [57], and the sleep–wake transition [16]. Although conventional critical indicators are analytically universal (close to the critical point, when noise is vanishingly small) and have been successfully applied to some real-world problems [17, 19, 40], they have yet to find widespread practical application in many noisy scenarios, such as predicting epileptic seizures [18, 58]. In real-world applications, the limitations of conventional critical indicators are tied to the need for quantitative accuracy despite a limited understanding of the system, in particular its stochastic components. Rather than looking for an increase in a statistical indicator of the DTC, tasks such as estimating the minutes until an epileptic seizure or the number of years until the collapse of an ecosystem require precisely calibrating the values of a critical indicator against a control parameter. Since properties such as standard deviation, autocorrelation, or skewness are highly sensitive to noise [45], the need for exact calibration is a point of failure for conventional indicators of criticality in systems where the strength of noise is unknown or variable. Dynamical noise—particularly when it has an unknown variance or distribution—is one of the major obstacles to applying universal theory and critical indicators derived for analytic systems to real-world scenarios involving finite, noisy time series.

To our knowledge, all conventional indicators of criticality are sensitive to noise. Some prior work has characterized how the strength of a noise process affects the time-series properties used to infer the control parameter, and therefore the DTC. Although scaling laws, which describe how the indicator varies with the control parameter, have been derived analytically for some indicators of criticality in low-noise cases, such scaling may not hold under moderate or high levels of noise. For instance, Meunier and Verga [56] demonstrated for the pitchfork bifur-

cation that features such as the Lyapunov exponent and autocorrelation no longer peak at the phenomenological bifurcation point in presence of additive noise. Instead, the peak of these time-series features (which marks a dynamical bifurcation point) is shifted along the control parameter to a degree that depends on the noise variance, thereby obscuring the critical point. Moreover, the splitting of the invariant density becomes less abrupt with increased noise, and other dynamical effects can occur after bifurcation of the underlying deterministic component [56, 59]. Even a recent measure, formulated to reliably signal the critical point across classes of bifurcations, is sensitive to dynamical noise [60].

While some studies have examined the behavior of critical indicators in systems with a given fixed noise level, prior work has yet to address the arguably more common real-world setting in which the noise amplitude is unknown and may vary (across different recordings of the system, or over instances of otherwise similar systems). This is a particularly challenging problem since knowledge of the noise process, especially its variance, is required to properly calibrate time-series features for meaningful prediction of the DTC. Additionally, established analytical tools that have been used to make progress in idealized cases cannot be applied straightforwardly to the variable-noise setting because their precise relationship to the control parameter depends on the noise amplitude. For example, two prototypical time-series indicators of the DTC—standard deviation and autocorrelation—both depend strongly on the strength of noise in the system: standard deviation increases with noise level, while autocorrelation decreases.

Given the ubiquity of systems corrupted by an uncertain amount of noise, it is of great importance to formulate robust indicators of the distance of such systems to nearby critical points. In this work, we introduce a data-driven methodology to tackle this problem, in which we simulate a noisy bifurcating system close to a critical point and then search across a large candidate library of time-series features, scoring each on how well it captures the DTC of a simulated system (Sec. II C). The most comprehensive collection of time-series features to date is the highly comparative time-series analysis library, *hctsa*, which contains over 7000 diverse features [61–63]. It contains measures of the distribution of time-series values, self-correlation properties, measures of predictability and complexity, methods related to self-similarity and recurrence properties derived from the literature on physics and nonlinear time-series analysis, among many others. Here, we address the challenge of inferring the DTC using the data-driven approach of identifying the most informative time-series features for a given criticality problem by searching across the *hctsa* feature set. To study how each time-series feature is influenced by dynamical noise, we consider our model system in two scenarios (Sec. II C): (i) the *fixed-noise* case in which the noise has a fixed strength; and (ii) the *variable-noise* case in which the noise amplitude varies across repeated mea-

surements of the system. By closely examining the types of features that covary strongly with the control parameter in the case of variable noise, we explain how these high-performing features combine the characteristics of noise-driven fast fluctuations with measurements taken from the stationary distribution (see Sec. III C). This combination enables a precise estimate of the shape of the potential—and hence an ability to track the DTC—despite the confound of uncertain noise amplitude.

The paper is structured as follows. In Sec. II, we introduce the supercritical Hopf normal form we use as a model critical system (in Sec. II A) and describe how we sampled noise and control parameters to generate a dataset of simulated time series (in Sec. II B). We detail our feature-extraction procedure and our scoring method for identifying high-performing features in the fixed-noise and variable-noise cases in Sec. II C. Next, in Sec. III, we reveal how well features across the *hctsa* library perform in the fixed-noise (Sec. III A) and variable-noise (Sec. III B) cases. After identifying the top-performing *hctsa* features in the variable-noise case and examining them in detail (Sec. III C), in Sec. III D we summarize the theoretical insight we gained from our data-driven approach and encapsulate our findings in a new time-series feature that can robustly track the DTC in near-critical systems with unknown noise amplitude. Finally, in Sec. IV we provide concluding remarks, discuss the implications of our findings for other noisy critical phenomena, and outline potential directions for future research.

II. METHODS

Here we outline our data-driven approach to finding useful statistical indicators of the DTC in the presence of dynamical noise in two cases: the *fixed-noise* case; and the *variable-noise* case. Our approach is shown schematically in Fig. 1, and can be summarized in two main steps: (i) simulate a time-series dataset from the normal form of a supercritical Hopf bifurcation [see Eq. (1), below], where each time series is generated using a specific control parameter (varying over a range up to the bifurcation point) and noise variance (either fixed, or varying over a specified range); and (ii) extract candidate features from each time series using the *hctsa* time-series feature library [61, 62] and score each feature on how well it tracks the control parameter μ across the dataset. In the fixed-noise case, the noise process has a constant strength, i.e., η is fixed for all time series in the dataset. By contrast, in the variable-noise case the noise amplitude can take a different value for any given time series; this setting models real-world situations in which the strength of noise might vary across different recordings of a system, or across different instances of similar systems.

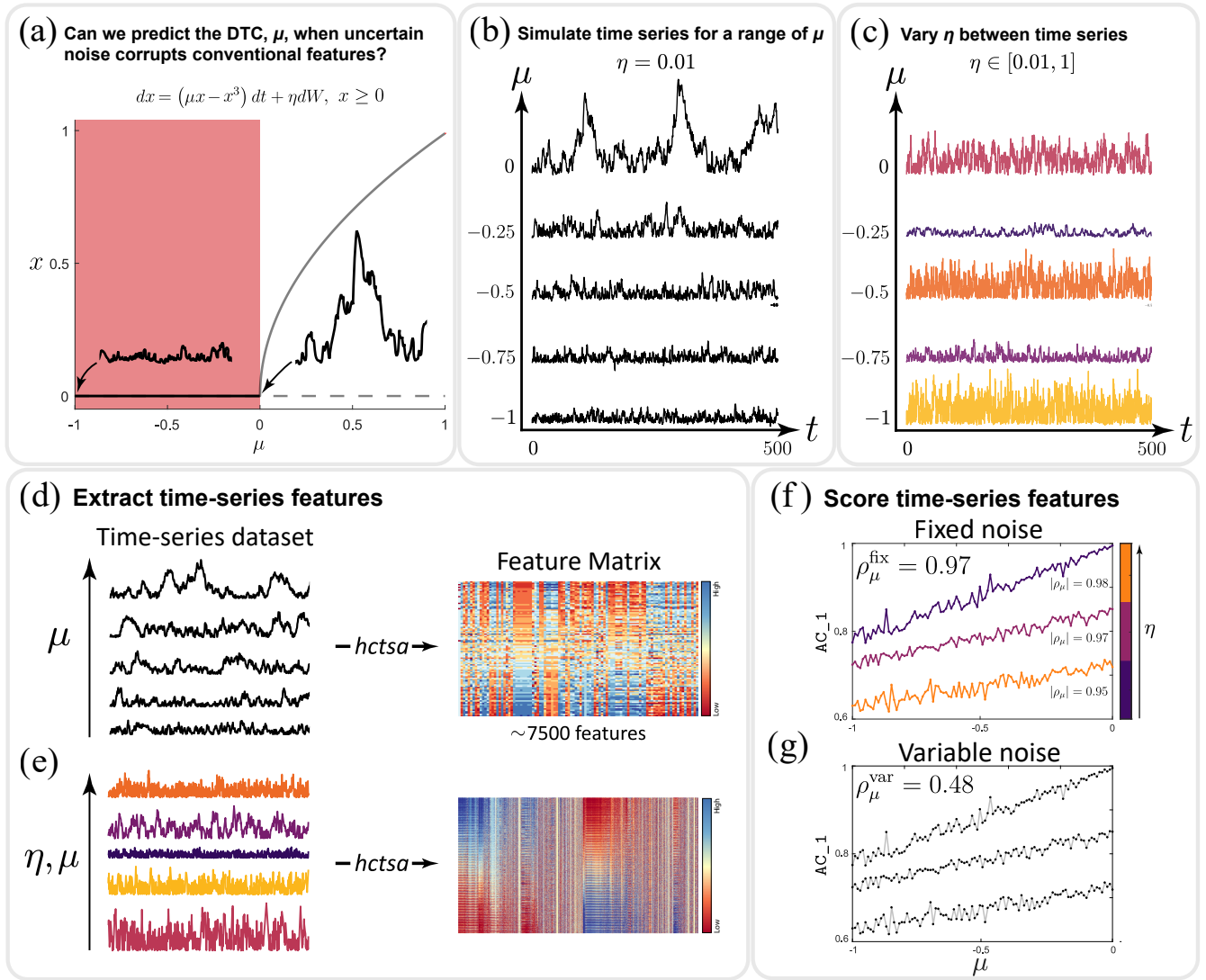


Figure 1: We take a data-driven approach to identifying time-series features that accurately track the distance to a critical point (DTC) of a noisy, near-critical system across a range of noise levels. (a) We investigate a model system close to the critical point: the radial component of the normal form for a supercritical Hopf bifurcation with $\mu < 0$, given by Eq. (1). A bifurcation diagram shows the radius of equilibrium points x , against the control parameter μ —when $\mu < 0$ (shaded red), there is a stable fixed point (solid black) at the origin. The model incorporates additive white Gaussian noise, given by dW , with a noise amplitude of η . We simulated time series across $-1 \leq \mu \leq 0$ and $0 < \eta \leq 1$. Snippets of representative time series are annotated. (b) Representative time series of 5000 samples for the fixed-noise problem, for which the noise level is fixed (shown here for $\eta = 0.01$), at selected values of $\mu = -1, -0.75, \dots, 0$. As μ approaches zero, it is visually clear that signal variance increases and fluctuations are slower. (c) Sample time series for the variable-noise problem: a different value of $0.01 \leq \eta \leq 1$ is chosen for each time series, but η is fixed over time. Relative to the fixed-noise case, the variable noise amplitude obscures the underlying variation in the control parameter μ . (d, e) To find time-series properties that are sensitive to μ in both the fixed-noise and variable-noise settings, we compared 7492 candidate time-series features using *hctsa* [62]. (d) The result of this feature extraction for a fixed value of η is depicted as a time series \times feature matrix, with rows ordered by μ . (e) The feature matrix for our full dataset, with variation in both μ and η , is depicted in the right panel, with rows ordered by η . (f, g) Finally, we scored each feature for its performance under the two conditions as ρ_{μ}^{fix} and ρ_{μ}^{var} . In the fixed-noise setting, (f), ρ_{μ}^{fix} was calculated as the magnitude of the correlation of a feature to μ for each value of $\eta = 0.01, 0.02, \dots, 1$ separately, and then averaged across all η values. In the variable-noise case (g), ρ_{μ}^{var} , was an overall correlation to μ after η labels had been discarded. An example is shown here for the autocorrelation at lag 1 (labeled AC_1), which is strongly correlated to μ for a given noise-level η (f) but only weakly correlated in the variable-noise case (g).

A. The model system

We first describe the model system used for generating time series at various distances, in the control parameter, from a critical point. We chose the radial component of the normal form for a supercritical Hopf bifurcation, as it applies to a broad range of real-world systems, including the wake-sleep transition [16], seizure dynamics [64], auditory hair cells [65, 66], financial markets [35], and many others [6, 7, 36, 67, 68]. Our system derives from the general normal form of a supercritical Hopf bifurcation [69], in which a stable fixed point bifurcates to a stable limit cycle and an unstable fixed point. Since noise often acts radially with a strength that is independent of the system’s phase, we chose to use the simplified radial component of the Hopf normal form, given by

$$dx = (\mu x - x^3) dt + \eta dW, \quad x \geq 0, \quad (1)$$

where W is a Wiener process. Notably, this resembles the normal form of pitchfork bifurcation with a reflecting boundary at the origin [6], permitting our results to generalize via a simple transformation to systems that exhibit pitchfork-type bifurcations (such as spin-glass systems [3] or models of epigenesis [70]). As shown in the bifurcation diagram in Fig. 1(a), a bifurcation occurs at the critical value, $\mu = 0$: for $\mu < 0$ there is a single stable fixed point at $x = 0$, whereas for $\mu > 0$ the origin is unstable. The corresponding potential function of this system, detailed in Sec. III C, is unimodal for $\mu < 0$, flattens as μ is increased to 0, and is bimodal for $\mu > 0$.

Here we consider the more complex problem of approaching the critical point from $\mu < 0$, corresponding to the regime with a single, stable fixed point where the system hovers near the origin [shaded in Fig. 1(a)]. We focus our study on this regime for three reasons. First, during events such as power-system failure [10, 11] and epileptic seizures [64] the fixed-point regime corresponds to safety, with the presence of low-power fluctuations, in contrast to the dangerous high-power oscillations that occur for $\mu > 0$. Second, the DTC is much more straightforward to estimate for $\mu > 0$: features that measure simple properties of the distribution, such as the mean or median, are insensitive to η when the noise amplitude is not large compared to the equilibrium radius [given by $\sqrt{\mu}$ for Eq. (1)]. Third, when the noise strength is large enough to mask changes in the distribution caused by varying $\mu > 0$, the system is already sufficiently close to the bifurcation point for the disappearance of the unstable branch to be insignificant.

B. Time-series simulation

To evaluate the performance of individual time-series features at tracking μ in the presence of a stochastic component with strength η , we simulated Eq. (1) in the range $-1 \leq \mu \leq 0$. We studied both the fixed-noise

and variable-noise scenarios with a combined time-series dataset generated by varying parameters across ranges $-1 \leq \mu \leq 0$ and $0 < \eta \leq 1$. In total, we simulated 10 100 time series, \mathbf{x} , using all combinations of 101 equally spaced values for $\mu = -1, -0.99, \dots, 0$, and 100 equally spaced values of $\eta = 0.01, 0.02, \dots, 1$. Time series were simulated using the Euler–Maruyama method [71] over 1000s with a time-step $dt = 10^{-3}$ s and an initial radius $x_1 = 0$. To avoid the effects of transient dynamics (which are sensitive to the initial condition), we discarded the first 500s of the integration period and down-sampled the remaining 500s to a sampling period of $\Delta t = 0.1$ s, yielding 5000-sample time series that were analyzed in the remainder of this work. From this combined dataset, we studied the fixed-noise case by searching for features that vary with μ when η is fixed, as depicted in Fig. 1(b). In the variable-noise case, depicted in Fig. 1(c), we searched for time-series features that vary with μ in a way that is consistent over confounding variation of η . Finally, note that our data-driven approach is focused on relatively short time series containing 5000 samples, in contrast to other studies that evaluate critical indicators on simulated data [60]. Representative examples of simulated time series are in Figs. 1(b) and 1(c).

C. Feature scoring

We next aimed to determine which types of time-series features, extracted from the noisy time series simulated above, could accurately track variations in the known parameter, μ . We achieved this in a data-driven way using a comprehensive collection of 7873 candidate time-series features from the highly comparative time-series analysis toolbox, *hctsa* (version 0.98) [61, 62]. Each time-series feature $f : \mathbb{R}^N \rightarrow \mathbb{R}$ maps an input time series (of $N = 5000$ samples here) to a single, real-valued summary statistic. The *hctsa* feature set contains methods developed across the interdisciplinary time-series analysis literature, including measures of outliers, periodicity, stationarity, predictability, self-affine scaling, and many others. We extracted all *hctsa* features from each simulated time series in the dataset described above. After feature extraction, we removed 381 features from our analysis that were not well-behaved across all time series (e.g., produced NaN values or constant outputs across the dataset), leaving 7492 good-quality features. The result of feature extraction across our full time-series dataset is visualized as a time series \times feature matrix in Fig. 1(e).

Our next goal was to assess the ability of each time-series feature to track the underlying variation of the control parameter μ across the time-series dataset described in Sec. II B. We scored each feature using a Spearman correlation coefficient ρ between its outputs across the dataset and the corresponding values of μ ; features with high $|\rho|$ strongly monotonically track the variation in μ . As depicted in Figs. 1(f) and 1(g), we considered the fixed-noise and variable-noise cases separately.

Table I: Summary of top-performing time-series features from the *hctsa* feature library. The magnitude of ρ_μ^{fix} and ρ_μ^{var} indicate how well each feature can track the distance to criticality in the fixed-noise and variable-noise settings, respectively. Our new features are `fitSupercriticalHopfRadius_1` and the rescaled auto-density (RAD), `CR_RAD_1`.

<i>hctsa</i> feature name	ρ_μ^{fix}	ρ_μ^{var}	Description
<code>standard_deviation</code>	0.98	0.23	Sample standard deviation.
<code>AC_1</code>	0.97	0.48	Lag-1 autocorrelation.
<code>DN_RemovePoints_max_01_ac1diff</code>	0.94	-0.88	Change in lag-1 autocorrelation from removing the largest 10% of values.
<code>SB_MotifTwo_mean_uu</code>	0.93	0.88	Proportion of pairs of consecutive values that are both above the mean.
<code>PP_Compare_rav2_kscn_olapint</code>	0.88	-0.87	Change in distribution after two-sample moving-average smoothing.
<code>ST_LocalExtrema_1100_meanrat</code>	0.91	-0.90	Ratio between the average maximum and minimum in 100-sample windows.
<code>fitSupercriticalHopfRadius_1</code>	0.92	-0.90	Potential function curve-fit to a kernel-density estimate of the density.
<code>CR_RAD_1 (RAD)</code>	0.93	0.93	Product of the spread of differences and tailedness of the distribution.

a. Fixed-noise case In the fixed-noise case, where the noise amplitude is constant across recordings, we analyzed subsets of time series with the same value of η . As depicted in Fig. 1(f), for each set of 100 time series with a given value of η , we calculated the Spearman correlation of each feature with μ (over $\mu = -1, -0.99, \dots, 0$). We then computed the *fixed-noise score* of a given feature, ρ_μ^{fix} , as the mean of these 100 Spearman correlation coefficients. That is, ρ_μ^{fix} measures the average performance of a time-series feature across many settings that each have a unique fixed noise level.

b. Variable-noise case In the variable-noise case, where the noise amplitude varies between recordings, we disregarded the η labels of each time series (treating them as unknown), as depicted in Fig. 1(g). We then computed the *variable-noise score* of a given feature, ρ_μ^{var} , as the Spearman correlation between the 10 100 feature values (over all time series) and the corresponding values of μ . That is, ρ_μ^{var} measures the performance in a single setting where the noise amplitude varies across time series.

III. RESULTS

By systematically exploring a supercritical Hopf bifurcation, our main aim was to investigate which types of time-series properties (from a diverse library of over 7000 candidates in *hctsa* [62]) accurately track the distance to criticality (DTC), given by $|\mu|$, in the pre-critical regime of $\mu < 0$. As detailed in Sec. II C above, features were scored based on their correlation to μ using either ρ_μ^{fix} , in the fixed-noise setting (Sec. III A), and, separately, ρ_μ^{var} , in the variable-noise setting (Sec. III B). In the variable-noise case, we find surprising types of features that strongly vary with the DTC. By examining the algorithmic elements that are common among these features and summarizing the theoretical insight they provide (Sec. III C), we develop a new time-series feature for tracking the DTC, which we name the *rescaled auto-density* (RAD; see Sec. III D).

A. The fixed-noise case

We first investigated the fixed-noise case, where individual features are scored according to their correlation with μ for a fixed noise level η . We quantified this correlation as ρ_μ^{fix} (an average of absolute Spearman correlation coefficients across each of 100 noise levels, η , cf. Sec. II C). We hypothesized that features that are well-known to track the vicinity of a system to a critical point—including measures of signal variance and autocorrelation—would receive high ρ_μ^{fix} scores. We also sought to investigate whether any new types of features show strong performance.

The distribution of ρ_μ^{fix} values across all 7492 time-series features is shown as a histogram in Fig. 2(a). We find many time-series features with strong performance on this fixed-noise task, e.g., 1348 of the 7492 tested features have $\rho_\mu^{\text{fix}} > 0.8$, and some features were scored as high as $\rho_\mu^{\text{fix}} = 0.98$. To more closely investigate the highest performing time-series features, we focused on the 100 features with $\rho_\mu^{\text{fix}} > 0.97$. We then sought to isolate groups of similarly behaving features from within this set of 100 features by computing pairwise Spearman correlation coefficients between all pairs of features (calculated using all time series), and reordering them using hierarchical linkage clustering. The results, shown in Fig. 2(b), reveal two distinct groups of high-performing features: one group measuring autocorrelation properties (annotated with an orange square), and another (smaller) group measuring properties of the distribution of time-series values, including mean and variance (annotated with a blue square).

The first cluster contains features that are sensitive to autocorrelation; all features in this cluster are highly correlated to lag-1 autocorrelation (*hctsa* feature name: `AC_1`), which has $\rho_\mu^{\text{fix}} = 0.97$. Disregarding the confounds of noise amplitude and the time step, lag-1 autocorrelation and other features that measure timescales of a system are sensitive to the critical slowing down that occurs close to the critical point [19]. As well as lag-1 autocorrelation, our data-driven analysis also reveals a range of conceptually related features that can

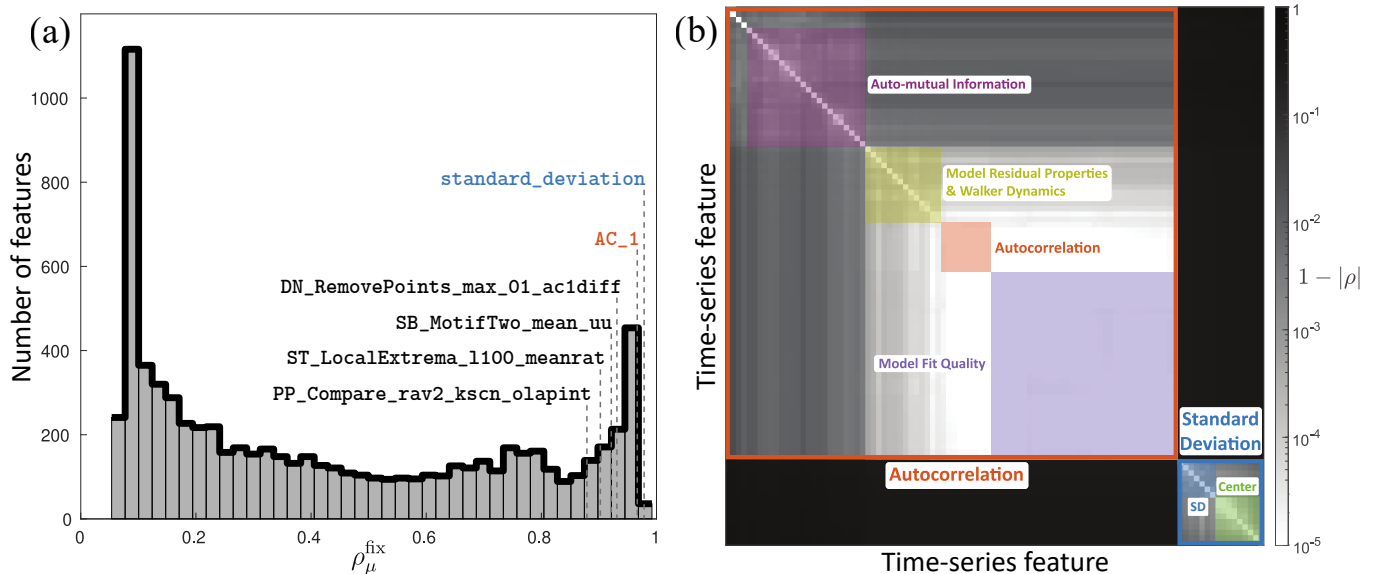


Figure 2: For a near-critical system with a fixed noise level, we recovered high-performing conventional statistical indicators of the distance to criticality by comparing the behavior of over 7000 candidate time-series features. (a) A histogram of fixed-noise feature scores, ρ_{μ}^{fix} , across 7492 time-series features (from the *hctsa* feature library).

Selected high-performing features are annotated, including standard deviation ($\rho_{\mu}^{\text{fix}} = 0.98$, labeled as `standard_deviation`, blue) and lag-1 autocorrelation ($\rho_{\mu}^{\text{fix}} = 0.97$, `AC_1`, red). Names of the top features for the variable-noise case are also annotated for comparison (cf. Fig. 3). (b) The top 100 features, with $\rho_{\mu}^{\text{fix}} \geq 0.97$, are plotted as a pairwise correlation matrix. The brightness of each element corresponds to the similarity between each pair of these features, using the metric $1 - |\rho|$, where ρ is the Spearman correlation coefficient. Rows and columns have been reordered to place similar features close to one another using average hierarchical linkage clustering (on Spearman correlation distances), revealing two clusters of features with common behavior which have been annotated using transparent colored squares. As labeled, the first cluster contains features measuring properties of signal autocorrelation (orange), while the second cluster contains features measuring properties related to the signal variance (blue). Features annotated in (a) are detailed in Table I, and for (b) a sorted list of features is provided in Supplemental Table S2.

also effectively capture the same variation in the self-correlation timescale, including measures of automutual information [72], properties of fitted autoregressive (AR) time-series model residuals, and others (see Supplemental Table S2 for a list of the top 100 fixed-noise features, clustered by similarity).

In the second cluster of features, which are related to the distribution of time-series values, the standard deviation (*hctsa* feature name: `standard_deviation`) displays very strong performance, with $\rho_{\mu}^{\text{fix}} = 0.98$. This is consistent with expectation—the potential function, described in Sec. III C, flattens when approaching a critical point, leading to higher-variance fluctuations for a given noise level η . Moreover, since the potential for our model system has a reflecting boundary at $x = 0$ [see Eq. (2)], we also find that measures of central tendency such as the mean, median, and root-mean-square, are highly correlated to the spread of the distribution (as captured by the standard deviation).

Our results have thus flagged two types of features that vary with the DTC, recapitulating prior literature

which has focused on critical slowing down (captured by measures of time-series autocorrelation [19], including the simple and effective indicator, lag-1 autocorrelation [12, 13, 40, 41, 46]) and fluctuations of increased variance (captured by the spread of the distribution of time-series values) [73] near a critical point. A complete list of *hctsa* features along with their fixed-noise scores, ρ_{μ}^{fix} , is in Supplemental Table S1.

B. The variable-noise case

Having established the ability of our data-driven approach to recapitulate a theoretical literature on time-series features for tracking the DTC in a system with fixed noise, we next investigated the more difficult problem of finding features that track the DTC in a variable-noise setting. We are unaware of prior work that has examined this relevant real-world scenario, which involves identifying statistical properties of time series that are sensitive to μ but insensitive to η . The lack of an *a priori*

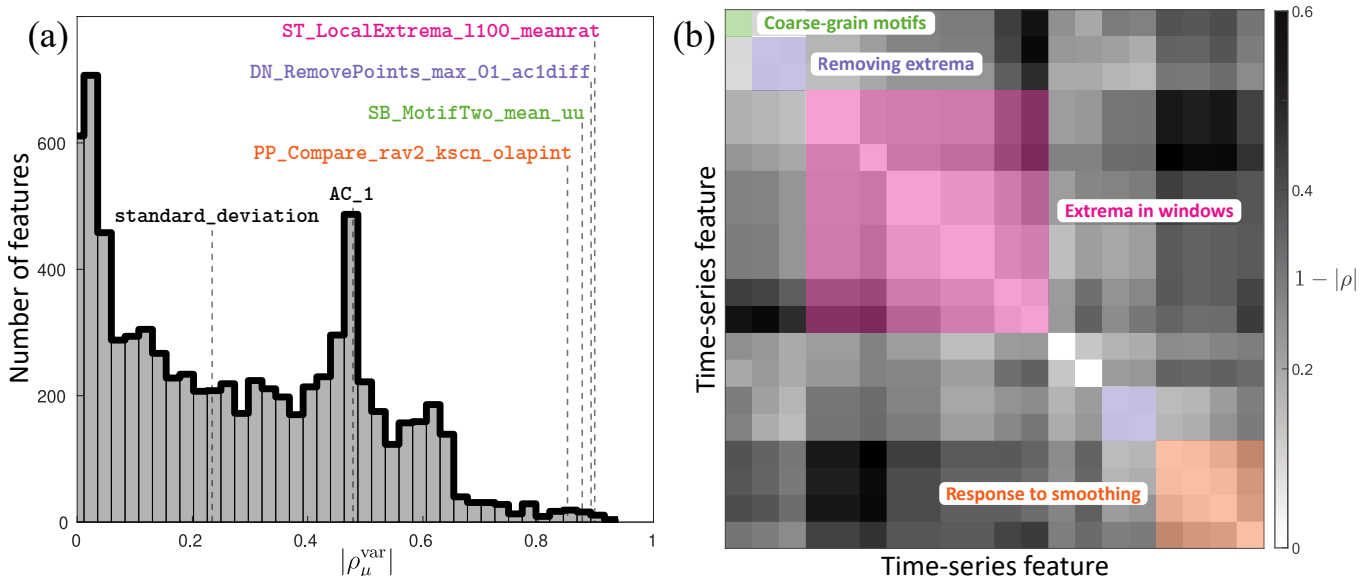


Figure 3: In the variable-noise setting, we identified a set of high-performing time-series features that measure properties of the distribution of time-embedded values. (a) A histogram of the variable-noise scores, $|\rho_\mu^{\text{var}}|$, is shown across all 7492 *hctsa* time-series features. Conventional indicators of criticality perform poorly, including standard deviation ($\rho_\mu^{\text{var}} = 0.23$, annotated as `standard_deviation`) and lag-1 autocorrelation ($\rho_\mu^{\text{var}} = 0.48$, annotated as `AC_1`). (b) The top 20 features in the variable-noise case ($|\rho_\mu^{\text{var}}| > 0.86$) are plotted in a pairwise correlation matrix, revealing many diverse clusters of features. Families of conceptually similar features are annotated, and the top features from outlined clusters were selected for closer study. Features annotated in (a) are detailed in Table I, and a sorted list of the features in (b) is in Supplemental Table S3.

understanding of how to construct a noise-level-robust indicator of the DTC from finite time series, and the difficulty (or intractability) of a direct analytical route to tackling the problem, makes it an ideal setting for our data-driven approach.

We computed the variable-noise performance score, ρ_μ^{var} , for all candidate time-series features in *hctsa* (full results are in Supplemental Table S1). The distribution of $|\rho_\mu^{\text{var}}|$ across all 7492 features is plotted in Fig. 3(a), including annotated scores of two selected features (the standard deviation and lag-1 autocorrelation). Reflecting the increased difficulty of the variable-noise setting, $|\rho_\mu^{\text{var}}|$ values are lower on average than ρ_μ^{fix} . We nevertheless observed a tail of high-scoring features; e.g., 49 time-series features have $|\rho_\mu^{\text{var}}| > 0.8$. As expected, the top-performing features in the fixed-noise case, including lag-1 autocorrelation (`AC_1`) and standard deviation (`standard_deviation`) are sensitive to both μ and η , and thus do not accurately track variation in μ in the presence of confounding variation in η . For example, for `standard_deviation`, $\rho_\mu^{\text{fix}} = 0.98$ (in the fixed-noise setting) drops to $\rho_\mu^{\text{var}} = 0.23$ (in the variable-noise setting), while for `AC_1`, $\rho_\mu^{\text{fix}} = 0.97$ drops to $\rho_\mu^{\text{var}} = 0.48$. To understand this behavior, we plotted the dependence of these two features as a function of μ for five selected noise levels in Figs. 4(a) and 4(b). We see that these features vary monotonically with μ for any given η value (under-

lying their strong fixed-noise performance), but they are highly sensitive to variation in η , making them unreliable indicators of the DTC in the variable-noise setting.

We next aimed to better understand the high-performing features that make up the right tail of Fig. 3(a). Focusing on the top twenty features, with $\rho_\mu^{\text{var}} > 0.86$, we plotted their pairwise distance matrix (on Spearman correlation distances, $1 - |\rho|$) in Fig. 3(b) (see Supplemental Table S3 for details on each cluster). One large family of highly correlated features examines how properties of extreme values within small windows (of ~ 100 samples) are distributed across the time series, such as the average ratio between the maximum and minimum value in each window [`ST_LocalExtrema_1100_meanrat`, shown in pink in Fig. 2(a)]. Other high-performing features include those that measure the change in autocorrelation after a proportion of time series extrema are removed (such as `DN_RemovePoints_max_01_ac1diff`, purple), the occurrence of simple motifs in a symbolization of the time series (i.e., transforming a sequence of real values to a symbolic string; `SB_MotifTwo_mean_uu`, green), or the change in the distribution of time-series values after smoothing the time series using a moving average (`PP_Compare_rav2_kscn_olapint`, orange).

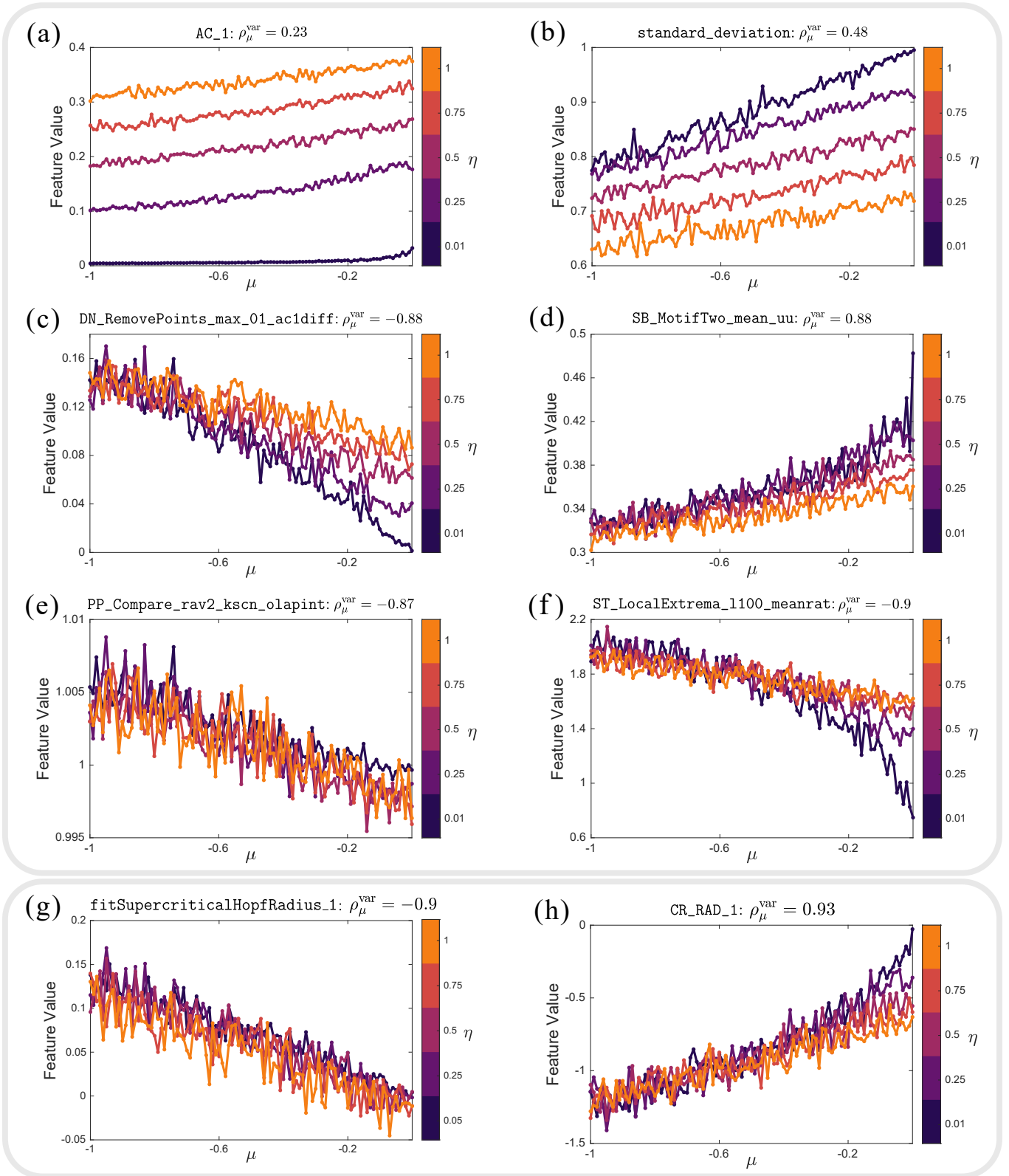


Figure 4: Conventional features for tracking the DTC only perform well in the fixed-noise setting, but we uncover new features that robustly track the DTC across different noise amplitudes. Feature values are plotted against μ for five values of the noise amplitude $\eta = 0.01, 0.25, 0.5, 0.75, 1$. Two of the top fixed-noise features, (a) standard deviation and (b) lag-1 autocorrelation, are highly correlated to μ for any given value of η (the fixed-noise case), but are poorly correlated across multiple η values (the variable-noise case). (c)–(f) The highest-performing time-series features in the variable-noise case are highly correlated to μ both within and across η values, demonstrating robust tracking of the DTC despite unknown noise amplitude. (g) A new feature introduced here, `fitSupercriticalHopfRadius_1`, distills the key algorithmic elements of the top-performing features. However, the curve-fitting algorithm is unstable for $\eta < 0.05$, so only $\eta = 0.05$ is shown for this feature. (h) A second new feature, RAD, uses elementary time-series operations to yield a computationally efficient and numerically stable estimate of the DTC. Each feature is summarized in Table I and detailed in Sec. III C.

C. Algorithmic steps underlying noise-robust features

In the previous section, we isolated a set of time-series features that can track the control parameter μ , while being minimally affected by changes in the noise level η , with a surprisingly strong correlation ($\rho_{\mu}^{\text{var}} > 0.86$). In this variable-noise setting, conventional indicators of the DTC, like standard deviation and lag-1 autocorrelation, perform poorly. In this section we aim to understand why these features perform so well. We are able to explain this by inspecting the algorithms underlying four of the highest-performing features, selected to represent the main clusters of high-performing feature behavior [in Fig. 3(b)]. These four features are named and briefly described in Table I and are annotated on Figs. 2(a) and 3(a), indicating their high performance in both the fixed-noise and variable-noise cases. Scatter plots of these features with μ for different noise levels, η , are shown in Figs. 4(c)–(f). Unlike the standard deviation [Fig. 4(a)] and lag-1 autocorrelation [Fig. 4(b)], these high-performing features vary strongly with μ in a similar way across noise levels, η , demonstrating their robustness to noise.

Despite appearing to be distinct features, close inspection of the algorithmic steps underlying each top feature revealed two key shared algorithmic components: (i) they involve estimating a statistic derived from the distribution of time-series values, such as a proportion of points within an interval of values; and (ii) they compare this statistic to the standard deviation of the incrementally differenced time series (a quantity that is closely related to the lag-1 autocorrelation). In this section we aim to summarize how these two algorithmic steps, which appear critical to the top-performing features, allow them to act as noise-robust estimators of the DTC. As with conventional metrics of criticality, such as standard deviation and autocorrelation, we notice that both algorithmic steps are closely related to a system’s potential function. By expressing these two properties in terms of the potential, we are able to explain how these features can successfully infer the DTC despite uncertain noise amplitude. We first derive the relationship between the potential and the two algorithmic steps: (i) the distribution of values; and (ii) the spread of differences.

a. The shape of the potential $V(x)$ depends on μ . The ability of some features to accurately track the DTC in the presence of uncertain noise amplitude can be understood in terms of the potential function of a system. The potential function of a stochastic system describes the effect of the deterministic components on the system dynamics: the gradient of the potential at a given point determines the rate of change due to the deterministic terms at that point [1]. In this formalism, the evolution of a system can be viewed intuitively as the trajectory of a heavily damped particle following the gradient of the potential toward a local minimum [1], in addition to any diffusive (or stochastic) drives. The potential formula-

tion provides a useful way of understanding critical slowing down and other conventional metrics of the DTC [40]. The potential function for the model system studied here is obtained by integrating Eq. (1), giving

$$V(x; \mu) = -\frac{\mu x^2}{2} + \frac{x^4}{4}, \quad x \geq 0. \quad (2)$$

As depicted in Figs. 5(a)–(d), as μ increases toward 0, $V(x)$ becomes shallower, reducing the restorative force toward the origin. This change in the shape of the potential results in dynamics with slower fluctuations (increased autocorrelation) and diffusion over a larger domain [increased standard deviation, cf. orange distributions in Figs. 5(a)–(d)]. However, Figs. 5(a)–(d) also show that η can make the relationship between the potential and autocorrelation or standard deviation ambiguous: the time-series autocorrelation takes a similar value for $\mu = -2, \eta = 0.5$ [Fig. 5(a)] as for $\mu = -0.1, \eta = 1.5$ [Fig. 5(d)], and the distribution has a similar standard deviation for $\mu = -2, \eta = 1.5$ [Fig. 5(b)] and $\mu = -0.1, \eta = 0.5$ [Fig. 5(c)]. While both the potential function and driving noise determine how a system evolves over time, we can see that a high-performing algorithm for estimating μ in the presence of variable noise should target a property that is specifically affected by μ : the shape of the potential function, $V(x; \mu)$.

b. The invariant density $p(x)$. Under the conceptual framing provided by the potential formulation, we next aimed to investigate whether the top-performing features are able to extract a noise-robust estimate of μ from time-series data by estimating the shape of the potential, $V(x; \mu)$. As described above, all top-performing features measure properties of the distribution, suggesting that this step may be relevant to robustly estimating the DTC (see Sec. III B). Following this connection, we investigated the invariant density $p(x)$: the probability density to which the distribution of values from a stationary system will converge over time. The invariant density is valuable for describing bifurcations when the abruptness of the qualitative change that occurs in the deterministic system is destroyed or smoothed by noise [56]. For a stationary system, the invariant density can be derived from the potential function and the noise term by taking the Fokker–Planck equation in the limit of infinite time [69]. For the system studied here, Eq. (1), the invariant density has the form

$$p(x; \mu, \eta) = A \exp\left(\frac{-2V(x; \mu)}{\eta^2}\right), \quad x \geq 0, \quad (3)$$

which is normalized to unit probability mass by A [56]. For fixed η , the potential can be inferred from the invariant density as

$$V(x; \mu) = -\frac{1}{2}\eta^2 [\ln p(x) - \ln A], \quad (4)$$

where it is straightforward to obtain an estimate of the probability density, $p(x)$, from measured data (e.g., using

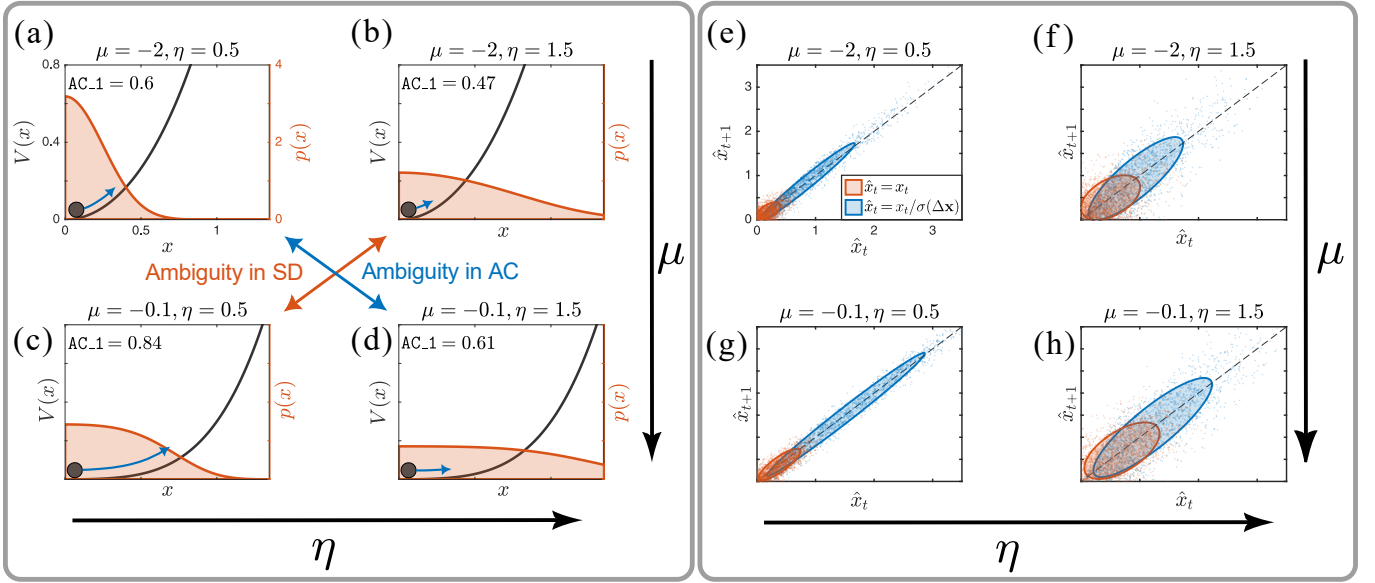


Figure 5: Rescaling time-series values by the spread of differenced values corrects for the confounding effect of a variable noise amplitude. (a)–(d) We plot the potential function, $V(x)$ (determined by the control parameter, μ , shown black), and distribution of values $p(x)$ (orange) for four combinations of μ and η : (a) $\mu = -2, \eta = 0.5$, (b) $\mu = -2, \eta = 1.5$, (c) $\mu = -0.1, \eta = 0.5$, and (d) $\mu = -0.1, \eta = 1.5$. The control parameter μ defines the DTC and determines the potential function, $V(x)$. The flatness of $V(x)$ gives rise to critical slowing down that, in combination with the noise amplitude η , determines $p(x)$ and the lag-1 autocorrelation (annotated as AC.1, top right). Both $p(x)$ and lag-1 autocorrelation values give ambiguous estimates of the DTC: different pairs of μ and η can result in the same feature value. (e)–(h) Scatters of (x_t, x_{t+1}) (orange) and the rescaled $(x_t/\sigma(\Delta \mathbf{x}), x_{t+1}/\sigma(\Delta \mathbf{x}))$ (blue) for the same four parameter settings as in (a)–(d): (e) $\mu = -2, \eta = 0.5$, (f) $\mu = -2, \eta = 1.5$, (g) $\mu = -0.1, \eta = 0.5$, and (h) $\mu = -0.1, \eta = 1.5$. After rescaling by the standard deviation in the $x_{t+1} - x_t$ direction, $\sigma(\Delta \mathbf{x})$ (described in Sec. III D), the distribution of $x_t + x_{t+1}$ becomes less sensitive to changes in the noise amplitude. Annotated ellipses indicate the covariance of (x_t, x_{t+1}) (orange), which is strongly affected by changes in η , but becomes more characteristic of μ after rescaling by $\sigma(\Delta \mathbf{x})$ (blue).

a kernel estimator [74]). Since Eq. (2), and therefore Eq. (4), depend on μ , time-series features that measure properties of the distribution of values in the time series (such as mean, standard deviation, and skewness) are able to provide accurate estimates of the DTC in the fixed- η case (as we verified in Sec. III A). However, as Eq. (4) depends strongly on η , features measuring the distribution of time-series values are highly sensitive to noise and thus have low ρ_μ^{var} (as we found in Sec. III B).

We now seek to incorporate the second algorithmic component of the top-performing features, the spread of differences, into our expression for the potential function, in the hope that it may eliminate the noise amplitude η from the invariant density and yield a noise-insensitive estimate of μ .

c. The spread of differences, $\sigma(\Delta \mathbf{x})$. In addition to the distribution of time-series values, the time-series features with the highest ρ_μ^{var} also indirectly measure the spread of the incrementally differenced time series $\Delta \mathbf{x}$, where Δ is the first difference operator and $\Delta x_t = x_t - x_{t-1}$ [75]. We write this spread here as $\sigma(\Delta \mathbf{x})$, where σ is the standard deviation (see Sec. S2 for fur-

ther details). Considering the drift and diffusion terms of Eq. (1), we see that the standard deviation of increments of the Wiener process scale with $\sqrt{\Delta t}$ [76], whereas increments of $(\mu x - x^3)dt$ scale with Δt . Hence for a small time step Δt the standard deviation of the differenced time series is dominated by the stochastic component ηdW . In the short-timestep limit, $\Delta t \rightarrow 0$, such that $\sqrt{\Delta t} \gg \Delta t$, we obtain an approximation for inferring η :

$$\sigma(\Delta \mathbf{x}) \approx \eta \sqrt{\Delta t}, \quad (5)$$

where $\sigma(\Delta \mathbf{x})$ is the standard deviation of the incrementally differenced time series $\Delta \mathbf{x}$.

The top-performing variable-noise features all involve measuring this dynamical quantity, $\sigma(\Delta \mathbf{x})$, that is informative of η . This insight allows us to understand how they may be able to eliminate the noise amplitude term from the invariant density to more accurately estimate the DTC. Incorporating this empirical estimate of η , from Eq. (5), into our expression for the potential in terms of the invariant density, Eq. (4), yields

$$V(x; \mu) \approx -\frac{\sigma^2(\Delta \mathbf{x})}{2\Delta t} [\ln p(x) - \ln A], \quad (6)$$

where we have assumed a fixed sampling period Δt .

To test Eq. (6), we used it to infer the DTC in the fixed-noise and variable-noise cases studied here. For the system given by Eq. (1), we can infer $V(x)\Delta t$, and therefore the DTC, using two properties that are easily measured from time-series data: the probability density $p(x)$ and the spread of differences $\sigma(\Delta\mathbf{x})$. The algorithmic procedure for inferring the DTC from data using Eq. (6) is as follows: i) produce a kernel-density estimate for $p(x)$; ii) calculate $\sigma(\Delta\mathbf{x})$ using the standard deviation and the first difference operator [75]; iii) transform the density to a potential using Eq. (6); iv) curve-fit Eq. (2) to the estimated potential; then v) infer μ by calculating the value of the second derivative at $x = 0$. We give this procedure the feature name `fitSupercriticalHopfRadius_1`, and show how it varies with both μ and η in Fig. 4(g).

Since `fitSupercriticalHopfRadius_1` varies strongly with the control parameter μ but minimally with the noise amplitude η , we find that it tracks the DTC in the variable-noise case far more strongly than conventional fixed-noise metrics, yielding scores that are on-par with the top-performing *hctsa* features (see Sec. III B): $\rho_{\mu}^{\text{fix}} = 0.92$ and $\rho_{\mu}^{\text{var}} = 0.90$ (see Supplemental Table S1 for a complete list of scores for both new features and *hctsa* features). The strong performance of `fitSupercriticalHopfRadius_1` suggests that Eq. (6) is indeed capturing key algorithmic principles relevant to robustly tracking the DTC. However, the top *hctsa* features (detailed in Sec. S2) are able to infer the DTC with disparate and often simple algorithms that do not rely on the computationally expensive steps of density estimation and curve fitting, and do not require explicitly knowing the form of the potential or the noise process. Furthermore, we found that `fitSupercriticalHopfRadius_1` suffers from numerical instability and produces noisy values when the noise amplitude is low, since the distribution is tightly concentrated around $x \approx 0$; in our simulations, this instability only occurred at $\eta = 0.01$. Armed with a theoretical explanation of how time-series features are able to estimate the DTC in the presence of noise, we next aimed to develop a simple, efficient, stable, and generic algorithm that implements the potential-based inference of the DTC described above.

D. Rescaled Auto-Density: a new noise-robust metric of the distance to criticality

In this section, we develop and test a new feature that directly implements the key algorithmic steps underpinning the success of the top-performing *hctsa* features, allowing us to efficiently estimate the DTC from data. We first detail a simplified approach to inferring the potential function $V(x)$ [cf. Eq. (6)] that eliminates η by rescaling time-series values by the standard deviation of incremental time-series differences, $\sigma(\Delta\mathbf{x})$. We then describe how the density of points in an (x_t, x_{t+1}) time-

delay embedding can be used to infer the DTC from the noise-robust rescaled potential. Finally, we introduce the Rescaled Auto-Density (RAD), a new time-series feature that uses elementary time-series operations to implement these key algorithmic principles.

a. Rescaled potential. We first notice that when the system is close to the origin, $x \ll 1$, the quadratic term in Eq. (2), $-\mu x^2/2$, dominates the quartic term $x^4/4$. Since our system is only driven by noise and has no extreme jumps or perturbations, it is naturally confined to a region close to the origin by the ‘steep walls’ of the quartic term [see Figs. 5(a)–(d)]. This behavior can be observed from the Taylor expansion of the invariant density, Eq. (3), given by

$$\tilde{p}(x; \mu, \eta) = B \left(1 + \mu \frac{x^2}{\eta^2} + \frac{\mu^2 x^4}{2 \eta^4} - \frac{x^4}{2\eta^2} + \mathcal{O}(x^6) \right), \quad (7)$$

where B is a constant that normalizes $\tilde{p}(x)$ to unit probability mass. Note, however, that this behavior breaks down when η becomes too large (the noise drives the system to extreme values where the quartic term dominates) or μ becomes too small (the quartic term dominates as the quadratic term is silenced). Under the approximation that the system tends to reside close to equilibrium, $x \ll 1$, we can write a simplified, rescaled potential as

$$\hat{V}(\hat{x}; \mu) = -\frac{\mu \hat{x}^2}{2} = -\frac{\ln[p(\hat{x})] - c}{2\Delta t}, \quad (8)$$

where $\hat{x} \geq 0$, c is a constant, and $\hat{x} = x/[\sigma(\Delta\mathbf{x})] \approx x/(\eta\Delta t)$. This approximate potential, \hat{V} , provides an algorithmically simpler way to estimate the DTC: we first rescale the system with $\hat{x} = x/[\sigma(\Delta\mathbf{x})]$ (aiming to eliminate the contribution of η) and then infer the potential of the rescaled system using the distribution of the rescaled values (to estimate μ). Unlike the theory described above, in Sec. III C, this simplified, highly approximate approach is not specific to the potential function of our model system.

b. The auto-density. Having identified a simpler method for ‘sensing’ the underlying potential function governing the deterministic dynamics, by rescaling the system with the standard deviation of incremental time-series differences, we now develop a simple algorithm for estimating the DTC from the inferred potential. We notice that the key attributes for robustly inferring the DTC—the invariant density and the spread of differences—can both be measured from the distribution of time-series values in an (x_t, x_{t+1}) time-delay embedding [77], as illustrated in Figs. 5(e)–(h). For the purposes of naming our feature, we refer to this two-dimensional distribution in (x_t, x_{t+1}) as the *auto-density* (in analogy to the autocorrelation). This auto-density captures the two properties we have found to be key for robustly inferring the DTC: the spread of differences, $\sigma(\Delta\mathbf{x})$, and the distribution, $p(x)$. First, in a two-dimensional embedding space, (x_t, x_{t+1}) , the factor $\sigma(\Delta\mathbf{x})$ is proportional to the standard deviation of shortest distances from $x_t = x_{t+1}$, or $x_{t+1} - x_t$. Second, when

the sampling period is small, $\Delta t \ll 1$, the distribution $p(x)$ is well approximated by the linear projection of x_t values onto the line defined by $x_t = x_{t+1}$, proportional to the distribution of the quantity $x_t + x_{t+1}$. The approximation given by Eq. (8) can then be implemented by rescaling x_t and x_{t+1} with the width of the auto-density in the $x_{t+1} - x_t$ direction. As illustrated in Figs. 5(e)–(h), rescaling the time-series values produces a distribution that is minimally sensitive to changes in the noise amplitude.

c. The rescaled auto-density. We now encapsulate the key algorithmic steps described above into a new time-series feature, RAD, that aims to robustly infer the DTC of noisy systems. It begins by partitioning the time-series values about a threshold that is insensitive to changes in extreme densities. The median (\tilde{x}) is a suitable choice for this threshold, partitioning the time series into two sets: time-series values above the median

$$U = \{x_t : x_t \geq \tilde{x}\}, \quad (9)$$

and the time-series values below the median

$$L = \{x_t : x_t < \tilde{x}\}. \quad (10)$$

RAD then aims to summarize of the shape of the invariant density while avoiding the need for the curve fitting (as required by `fitSupercriticalHopfRadius_1`, cf. Sec. III C). For a simple measurement of the shape of the probability density, we quantify the tailedness as the difference in the average density between the upper and lower partitions. Here we define the average density in each partition as the ratio of the probability mass contained in the partition and the width of the partition, measured by the standard deviation. Noting that the two partitions are split by the median, and therefore have an equal probability mass of 0.5, we can capture the average density in a partition as the inverse of the standard deviation, $1/\sigma$. Rescaling the difference between the average densities of the upper and lower partitions (which measures the shape of the distribution, in particular the higher-order moments) by $\sigma(\Delta \mathbf{x})$ completes our RAD feature, which is then given by

$$f_{\text{RAD}} = \sigma(\Delta \mathbf{x}) \left[\frac{1}{\sigma(U)} - \frac{1}{\sigma(L)} \right]. \quad (11)$$

To verify the DTC-tracking performance of RAD, we applied it to the fixed-noise and variable-noise cases analyzed above, as shown in Fig. 4(h). In the variable-noise case, RAD out-performed all other *hctsa* features, with $\rho_\mu^{\text{fix}} = 0.93$ (see `CR_RAD_1` in Supplemental Table S1). RAD also exhibits competitive performance relative to the top features in the fixed-noise setting, with $\rho_\mu^{\text{var}} = 0.93$. RAD is a straightforward and transparent algorithm that behaves as a reliable indicator of DTC in noisy systems. An implementation of RAD is provided in an accompanying Matlab code repository [78], and is included in the *hctsa* time-series feature library.

IV. DISCUSSION

This work addresses the challenge of estimating the distance to a critical point, DTC, in the presence of an uncertain, and potentially variable, confounding noise amplitude. While many studies have tackled the challenge of describing how noise disrupts conventional metrics of the DTC [12, 13, 45, 56], to our knowledge no work has attempted to identify new features that are insensitive to changes in the noise level. Moreover, our work demonstrates the ability of our novel data-driven methodology to motivate new theory and algorithmic implementations relevant to working with real (finite and noisy) time series. Specifically, by comparing the performance of thousands of time-series analysis features, we identified novel analysis methods that were able to robustly track the DTC in systems with variable levels of dynamical noise. By analyzing the algorithmic steps underlying top-performing time-series features, we developed a deeper theoretical understanding. This knowledge enabled us to reverse-engineer a novel, efficient, and noise-robust index of the DTC that out-performs all other *hctsa* features on this problem: the rescaled auto-density, RAD.

Our data-driven approach to solving theory-based problems is highly flexible, and could be extended to many real-world problems, particularly those involving short, noisy time-series data. The approach involves first simulating a known dynamical mechanism (to generate time-series data with a known structure), and then searching across a sufficiently large and comprehensive set of candidate time-series features for those that can best recover the underlying structure. This highly comparative methodology has been used previously by Fulcher *et al.* [61] to find statistical estimators of the scaling exponent of self-affine time series, and the Lyapunov exponent of Logistic Map time series; problems for which high-performing features were known to exist within the candidate feature set. This is also the case for the first fixed-noise setting investigated here, where our data-driven approach recapitulated the strong performance of conventional criticality metrics related to autocorrelation and the distribution of values. However, here we also extended it to a new setting, the variable-noise setting, in which it was not known whether any features would exhibit strong performance. We demonstrated that conventional metrics with high ρ_μ^{fix} (that correlate strongly with the DTC in the fixed-noise setting) perform poorly in this variable-noise setting, exhibiting low ρ_μ^{var} (Sec. III B). But, surprisingly, we identified several high- ρ_μ^{var} features that can track DTC in the presence of confounding variations in noise amplitude.

Having identified noise-robust features of DTC from *hctsa*, we then showed how our data-driven methodology can motivate the development of new theory and understanding. In this capacity, our approach sits alongside recent efforts to generate practical understanding from data using interpretable machine-learning algorithms [79, 80] or to solve analytical problems using ar-

tificial intelligence [81]. Unlike existing approaches, our methodology uses a simple search across a comprehensive library of transparent algorithms drawn from existing literature, automatically flagging those that are relevant to a given problem. Studying the highlighted algorithms can then yield new theoretical insight into the problem at hand. In this work, noticing key algorithmic similarities in the top-performing features motivated us to develop a theoretical account of how these algorithmic steps were able to track DTC so successfully. The resulting theory (invoking a potential formulation, Eq. (2) and corresponding expression for the invariant density, Eq. (3)) was used to formulate a new high-performing time-series feature, RAD, that robustly infers the shape of the potential function, which depends only the DTC, by measuring the time-series distribution after rescaling values with the spread of differences (see Sec. III D). RAD had a higher correlation to the DTC than other features in the variable-noise setting, while also performing similarly well in the fixed-noise case, making it a highly practical candidate statistic for tracking the DTC in real-world settings. Given the increasingly broad and detailed datasets being generated across scientific domains, this work thus demonstrates an ability to derive theoretical insight and develop practical analytic tools via the broad algorithmic comparison enabled by large algorithmic libraries like *hctsa* [62]. Our approach serves as a model for using wide methodological comparison to tackle similar problems that aim to develop new theory for bridging dynamical mechanisms with the statistical properties, such as criticality, that are most sensitive to the theoretical structures of interest.

No prior studies have tackled the challenge of developing noise-robust indicators of the DTC by distilling theory from a data-driven exploration. However, the algorithmic components of RAD, including the spread of differences and a measurement of asymmetry in the distribution, Eq. (11), share similarities with existing metrics related to criticality. For instance, the spread of differences (see Sec. III C) has been used to anticipate critical transitions in cryptocurrency markets [82], whereas skewness and related properties of the distribution (see Sec. III C) have been used to mark abrupt changes in ecosystems [83] and climates [84]. Crucially, neither the spread of differences nor the distribution alone give noise-robust features. As we highlight here, the confounding influence of the noise amplitude can only be eliminated by carefully combining these two properties (see Sec. III D). Furthermore, estimating the DTC typically requires precisely calibrating a feature against the control parameter and the noise amplitude through repeated observation on a system-by-system basis. Although RAD still requires calibration to the control parameter, unlike typical indicators of the DTC, there is no need to re-calibrate for changes or uncertainty in noise (e.g. see Fig. S1(b) for an illustration of how concrete predictions of the DTC can be made using linear fits of the top variable-noise *hctsa* features). RAD also has many other advantages

over other existing critical indicators that have been applied in noisy settings, including: (i) it does not require perturbing the system [85]; (ii) it operates on univariate time series [49]; and (iii) it performs well on short time series (but assumes a small sampling period). Many real-world systems are corrupted by noise with an unknown strength, can only be recorded for short periods, and cannot be measured in their full multivariate complexity. As such, RAD may improve accuracy in the wide range of tasks that involve quantitatively anticipating criticality from time-series data.

Even though our data-driven methodology for finding noise-robust features can be generically applied to various critical systems, we have made a number of simplifying choices that limit how well RAD will perform on arbitrary critical systems. Foremost, we chose to examine a simple normal form [see Sec. II A and Eq. (1)] that describes a broad range of systems, from auditory hair cells [65, 66] to financial markets [35], and many others [6, 67]. Features that perform well for Eq. (1) can be adapted for the full form of the Hopf bifurcation by calculating the radius, and for the pitchfork bifurcation by taking the absolute value. Although numerical simulations were only performed for Eq. (1), we expect our summary feature to perform well on other systems that exhibit a Hopf or pitchfork bifurcation. However, other normal forms can exhibit fundamentally different changes during bifurcation than the Hopf or pitchfork normal forms. The saddle-node normal form, for instance, occurs when an unstable and a stable equilibrium annihilate one another. In this case, the potential grows more asymmetric as the critical point is approached: unless the noise is sufficiently weak the DTC is large, RAD is unlikely to remain noise-robust for saddle-node bifurcations (and other systems with asymmetric normal forms, such as for transcritical bifurcations). Furthermore, many systems—such as the saddle-node, transcritical, and subcritical Hopf or pitchfork bifurcations [12]—exhibit critical transitions in which proximity to the critical point corresponds to explosive jumps toward distant attractors. For these systems, time-series features are unable to give a deterministic estimate of the time to catastrophe at high values of η , since crossings of the unstable threshold can be induced by noise well before the critical point [12]. The DTC is still a useful quantity, however, for inferring the likelihood of a critical transition, and given that most potential functions are locally quadratic around stable fixed points we expect RAD to generically out-perform conventional metrics under variable-noise conditions, in particular for subcritical Hopf and pitchfork bifurcations. Applying our data-driven methodology to find the most noise-robust DTC indicators for new normal forms is a promising avenue for future work, along with using our approach across classes of bifurcations to find a critical indicator that is not only noise-robust, but remains consistent over classes of bifurcations [60].

In addition to a simple deterministic component, we have also considered a highly simplified noise process.

Additive dynamical noise, which here is Gaussian, independent, and identically distributed, appears in many systems and is a common modelling assumption. Unlike measurement noise, which is incorporated into the signal after a system has evolved and been measured, dynamical noise is present in the equations of motion for a system, and continually interplays with the deterministic dynamics controlled by the potential function. However, critical systems can possess colored, correlated, or non-Gaussian noise [59, 86], multiplicative noise, or even noise in the control parameter itself [6]; we did not study such cases here. Moreover, we did not aim to find features that are insensitive to variation in both the noise amplitude and the sampling period, although we expect this to be a more difficult problem. It is also crucial to recognize the difference between noise with an unknown or uncertain strength, as treated in this work, and noise with a fast, time-dependent strength, which would certainly interfere with all of our noise-robust features. Regardless, we expect our results will generalize well to systems that: i) are near Hopf or pitchfork bifurcations; ii) are sufficiently close to a potential minimum, with no extreme perturbations; and iii) have a noise level small enough for the system to remain localised around a single potential minimum. For systems outside of this regime, the methodology we used to develop our summary feature—performing a data-driven exploration of candidate features to uncover new theoretical principles—is viable for phase transitions and noise processes of other varieties, and is a promising avenue for future scientific work.

Given the inherent stochasticity and complexity of real-world critical systems, accurately tracking the DTC using statistical properties of time-series data poses a significant challenge, prompting interdisciplinary research efforts spanning several decades. Most work has relied on two substantial assumptions: that the DTC is small enough for the theory of normal forms to apply, and that the dynamical noise is negligible or fixed. However, conventional metrics of the DTC are highly sensitive to the

more realistic setting of variable, or uncertain, noise. In this work, we have used a powerful and thorough data-driven approach that surveys a vast library of time-series features to: i) confirm that conventional metrics are disrupted by a variable noise amplitude; ii) uncover unstudied time-series features that are insensitive to the noise amplitude; iii) scrutinize these noise-robust features to develop new theoretical insight; and iv) summarize our new understanding into a simple new feature for accurately inferring the DTC in noisy real-world systems.

This work thus demonstrates a pragmatic, data-driven way of understanding theoretical systems through simulated data and wide methodological comparison, which can automatically flag promising algorithms to motivate the development of new theory. The result of this process, RAD, introduced here, is a viable measure of DTC for realistic settings of systems corrupted by unknown, and in general variable, noise amplitude. We expect these innovations to enable new applications of dynamical systems thinking to noisy, real-world systems.

Code availability

Matlab code for reproducing our simulations and analyses is available at the [Criticality](#) repository on GitHub [78]. This Matlab repository includes a script to reproduce the key figures from this paper as well as functions for `CR_RAD_1` (located in the file `RAD.m`) and `fitSupercriticalHopfRadius_1` (at `potentialDistributions.m`). RAD is available as the `CR_RAD` function in *hctsa* v1.08 [87] and the `Catch22.jl` Julia package [78]. RAD is also included in the default set of *hctsa* features as `CR_RAD_1` (RAD using the standard deviation of lag-1 differences), `CR_RAD_2` (RAD with lag-2 differences) and `CR_RAD_tau` (RAD using differences at a lag equal to the first zero-crossing of the autocorrelation function).

-
- [1] S. H. Strogatz, *Nonlinear dynamics and chaos: with applications to physics, biology, chemistry and engineering*, first edition ed. (Perseus Books Publishing, 1994).
 - [2] T. Ma, S. Wang, T. Ma, and S. Wang, Equilibrium phase transitions in statistical physics, in *Phase Transition Dynamics* (Springer International Publishing, Cham, 2019) pp. 129–278.
 - [3] J. M. Carlson, J. T. Chayes, L. Chayes, J. P. Sethna, and D. J. Thouless, Bethe lattice spin glass: The effects of a ferromagnetic bias and external fields. i. bifurcation analysis, *Journal of Statistical Physics* , 987 (1990).
 - [4] A. Mazumdar and G. White, Review of cosmic phase transitions: their significance and experimental signatures, *Reports on Progress in Physics* , 076901 (2019).
 - [5] M. A. Muñoz, Colloquium: Criticality and dynamical scaling in living systems, *Reviews of Modern Physics* **90**, 551 (2018).
 - [6] F. Freyer, J. A. Roberts, P. Ritter, and M. Breakspear, A canonical model of multistability and scale-invariance in biological systems, *PLOS Computational Biology* **8**, e1002634 (2012).
 - [7] L. Cocchi, L. L. Gollo, A. Zalesky, and M. Breakspear, Criticality in the brain: A synthesis of neurobiology, models and cognition, *Progress in Neurobiology* **158**, 132 (2017).
 - [8] G. Chen and P. Gong, Computing by modulating spontaneous cortical activity patterns as a mechanism of active visual processing, *Nature Communications* **10**, 4915 (2019).
 - [9] A. J. Fontenele, N. A. P. de Vasconcelos, T. Feliciano, L. A. A. Aguiar, C. Soares-Cunha, B. Coimbra, L. Dalla Porta, S. Ribeiro, A. J. a. Rodrigues, N. Sousa, P. V. Carelli, and M. Copelli, Criticality between cortical states, *Phys. Rev. Lett.* **122**, 208101 (2019).

- [10] V. Ajarapu and B. Lee, Bifurcation theory and its application to nonlinear dynamical phenomena in an electrical power system, *IEEE Transactions on Power Systems* **7**, 424 (1992).
- [11] K. N. Srivastava and S. C. Srivastava, Application of hopf bifurcation theory for determining critical value of a generator control or load parameter, *International Journal of Electrical Power & Energy Systems* **17**, 347 (1995).
- [12] C. Kuehn, A mathematical framework for critical transitions: Bifurcations, fast–slow systems and stochastic dynamics, *Physica D: Nonlinear Phenomena* **240**, 1020 (2011).
- [13] C. Kuehn, A mathematical framework for critical transitions: Normal forms, variance and applications, *Journal of Nonlinear Science* **23**, 457 (2013).
- [14] R. D. Peters, M. Le Berre, and Y. Pomeau, Prediction of catastrophes: An experimental model, *PRE* **86**, 026207 (2012).
- [15] A. J. K. Phillips and P. A. Robinson, A quantitative model of sleep-wake dynamics based on the physiology of the brainstem ascending arousal system, *Journal of Biological Rhythms* **22**, 167 (2007).
- [16] D.-P. Yang, L. McKenzie-Sell, A. Karanjai, and P. A. Robinson, Wake-sleep transition as a noisy bifurcation, *Phys. Rev. E* **94**, 022412 (2016).
- [17] M. I. Maturana, C. Meisel, K. Dell, P. J. Karoly, W. D'Souza, D. B. Grayden, A. N. Burkitt, P. Jiruska, J. Kudlacek, J. Hlinka, M. J. Cook, L. Kuhlmann, and D. R. Freestone, Critical slowing down as a biomarker for seizure susceptibility, *Nature Communications* **11**, 2172 (2020).
- [18] S. Liu, F. Li, and F. Wan, Distance to criticality undergoes critical transition before epileptic seizure attacks, *Brain Research Bulletin* **200**, 110684 (2023).
- [19] V. Dakos, M. Scheffer, E. H. van Nes, V. Brovkin, V. Petoukhov, and H. Held, Slowing down as an early warning signal for abrupt climate change, *Proceedings of the National Academy of Sciences* **105**, 14308 (2008).
- [20] M. Gleiser, E. W. Kolb, and R. Watkins, Phase transitions with sub-critical bubbles, *Nuclear Physics B* , 411 (1991).
- [21] L. Reatto, A complex view of criticality, *Nature Physics* **3**, 594 (2007).
- [22] A. Kianercy, R. Veltri, and K. J. Pienta, Critical transitions in a game theoretic model of tumour metabolism, *Interface Focus* **4** (2014).
- [23] C. Trefois, P. M. A. Antony, J. Goncalves, A. Skupin, and R. Balling, Critical transitions in chronic disease: transferring concepts from ecology to systems medicine, *Current Opinion in Biotechnology* **34**, 48 (2015).
- [24] A. S. Gsell, U. Scharfenberger, D. Özkundakci, A. Walters, L.-A. Hansson, A. B. G. Janssen, P. Nöges, P. C. Reid, D. E. Schindler, E. Van Donk, V. Dakos, and R. Adrian, Evaluating early-warning indicators of critical transitions in natural aquatic ecosystems, *Proceedings of the National Academy of Sciences* **113**, E8089 (2016), <https://www.pnas.org/content/113/50/E8089.full.pdf>.
- [25] E. Cotilla-Sanchez, P. D. H. Hines, and C. M. Danforth, Predicting critical transitions from time series synchrophasor data, *IEEE Transactions on Smart Grid* , 1832 (2012).
- [26] L.-W. Kong, H.-W. Fan, C. Grebogi, and Y.-C. Lai, Machine learning prediction of critical transition and system collapse, *Phys. Rev. Res.* **3**, 013090 (2021).
- [27] H. Ren and D. Watts, Early warning signals for critical transitions in power systems, *Electric Power Systems Research* **124**, 173 (2015).
- [28] T. M. Lenton, Early warning of climate tipping points, *Nature Climate Change* **1**, 201 (2011).
- [29] C. W. Lynn and D. S. Bassett, The physics of brain network structure, function and control, *Nature Reviews Physics* **1**, 318 (2019).
- [30] Y. A. Kuznetsov, Elements of applied bifurcation theory, *Applied Mathematical Sciences* **10.1007/978-1-4757-3978-7** (2004).
- [31] L. Zhang, C. Zhang, and Z. He, Codimension-one and codimension-two bifurcations of a discrete predator–prey system with strong allee effect, *Mathematics and Computers in Simulation* **162**, 155–178 (2019).
- [32] C. Meisel, A. Klaus, C. Kuehn, and D. Plenz, Critical slowing down governs the transition to neuron spiking, *PLOS Computational Biology* **11**, e1004097 (2015).
- [33] S. Rau, J. Main, P. Köberle, and G. Wunner, Pitchfork bifurcations in blood-cell-shaped dipolar bose-einstein condensates, *Physical Review A* **81**, 031605 (2010).
- [34] O. V. Ushakov, H.-J. Wünsche, F. Henneberger, I. A. Khovanov, L. Schimansky-Geier, and M. A. Zaks, Coherence resonance near a hopf bifurcation, *Physical Review Letters* **95**, 123903 (2005).
- [35] Q. Gao and J. Ma, Chaos and hopf bifurcation of a finance system, *Nonlinear Dynamics* **58**, 209 (2009).
- [36] A. Hudspeth, Integrating the active process of hair cells with cochlear function, *Nature Reviews Neuroscience* **15**, 600 (2014).
- [37] J. D. Victor, J. D. Drover, M. M. Conte, and N. D. Schiff, Mean-field modeling of thalamocortical dynamics and a model-driven approach to eeg analysis, *Proceedings of the National Academy of Sciences* **108**, 15631–15638 (2011).
- [38] K. M. Aquino, B. Fulcher, S. Oldham, L. Parkes, L. Gollo, G. Deco, and A. Fornito, On the intersection between data quality and dynamical modelling of large-scale fmri signals, *NeuroImage* **256**, 119051 (2022).
- [39] J. D. Crawford, Introduction to bifurcation theory, *Reviews of Modern Physics* **63**, 991 (1991).
- [40] M. Scheffer, S. R. Carpenter, T. M. Lenton, J. Bascompte, W. Brock, V. Dakos, J. Van De Koppel, I. A. Van De Leemput, S. A. Levin, E. H. Van Nes, M. Pascual, and J. Vandermeer, Anticipating critical transitions, *Science* **338**, 344 (2012).
- [41] M. Scheffer, J. Bascompte, W. A. Brock, V. Brovkin, S. R. Carpenter, V. Dakos, H. Held, E. H. van Nes, M. Rietkerk, and G. Sugihara, Early-warning signals for critical transitions, *Nature* **461**, 53 (2009).
- [42] Y. Hart, M. Vaziri-Pashkam, and L. Mahadevan, Early warning signals in motion inference, *PLOS Computational Biology* **16**, e1007821 (2020).
- [43] C. Wissel, A universal law of the characteristic return time near thresholds, *Oecologia* **65**, 101 (1984).
- [44] E. Negahbani, D. A. Steyn-Ross, M. L. Steyn-Ross, M. T. Wilson, and J. W. Sleigh, Noise-induced precursors of state transitions in the stochastic wilson-cowan model, *The Journal of Mathematical Neuroscience* (2015).
- [45] S. M. O'Regan and D. L. Burton, How stochasticity influences leading indicators of critical transitions, *Bulletin of Mathematical Biology* **80**, 1630 (2018).

- [46] V. Dakos, E. H. van Nes, P. D’Odorico, and M. Scheffer, Robustness of variance and autocorrelation as indicators of critical slowing down, *Ecology* **93**, 264 (2012).
- [47] S. R. Carpenter, J. J. Cole, M. L. Pace, R. Batt, W. A. Brock, T. Cline, J. Coloso, J. R. Hodgson, J. F. Kittell, D. A. Seekell, L. Smith, and B. Weidel, Early warnings of regime shifts: A whole-ecosystem experiment, *Science* **332**, 1079 (2011).
- [48] V. Dakos, E. H. van Nes, R. Donangelo, H. Fort, and M. Scheffer, Spatial correlation as leading indicator of catastrophic shifts, *Theoretical Ecology* **3**, 163–174 (2009).
- [49] E. Weinans, R. Quax, E. H. van Nes, and I. A. v. d. Leemput, Evaluating the performance of multivariate indicators of resilience loss, *Scientific Reports* **11**, 10.1038/s41598-021-87839-y (2021).
- [50] J. Liu, Y. Tao, R. Lan, J. Zhong, R. Liu, and P. Chen, Identifying the critical state of cancers by single-sample markov flow entropy, *PeerJ* **11**, e15695 (2023).
- [51] L. Arnold, *Random Dynamical Systems*, Monographs in Mathematics (Springer, 1998).
- [52] M. Siefert, A. Kittel, R. Friedrich, and J. Peinke, On a quantitative method to analyze dynamical and measurement noise, *Europhysics Letters (EPL)* **61**, 466–472 (2003).
- [53] T. Sase, J. P. Ramírez, K. Kitajo, K. Aihara, and Y. Hirata, Estimating the level of dynamical noise in time series by using fractal dimensions, *Physics Letters A* **380**, 1151–1163 (2016).
- [54] H. Crauel and F. Flandoli, Additive noise destroys a pitchfork bifurcation, *Journal of Dynamics and Differential Equations* **10**, 259 (1998).
- [55] M. Callaway, T. S. Doan, J. S. W. Lamb, and M. Rasmussen, The dichotomy spectrum for random dynamical systems and pitchfork bifurcations with additive noise, *Ann. Inst. H. Poincaré Probab. Statist.* **53**, 1548 (2017).
- [56] C. Meunier and A. D. Verga, Noise and bifurcations, *Journal of Statistical Physics* **50**, 345 (1988).
- [57] J. M. T. Thompson and J. Sieber, Predicting climate tipping as a noisy bifurcation: a review, *International Journal of Bifurcation and Chaos* **21**, 399 (2011).
- [58] T. Wilkat, T. Rings, and K. Lehnertz, No evidence for critical slowing down prior to human epileptic seizures, *Chaos* **29**, 091104 (2019).
- [59] L. Fronzoni, R. Mannella, P. V. E. McClintock, and F. Moss, Postponement of hopf bifurcations by multiplicative colored noise, *Physical Review A* **36**, 834 (1987).
- [60] F. Grziwotz, C.-W. Chang, V. Dakos, E. H. van Nes, M. Schwarzländer, O. Kamps, M. Heßler, I. T. Tokuda, A. Telschow, and C.-h. Hsieh, Anticipating the occurrence and type of critical transitions, *Science Advances* **9**, 10.1126/sciadv.abq4558 (2023).
- [61] B. D. Fulcher, M. A. Little, and N. S. Jones, Highly comparative time-series analysis: the empirical structure of time series and their methods, *Journal of The Royal Society Interface* **10** (2013).
- [62] B. D. Fulcher and N. S. Jones, hctsa: A computational framework for automated time-series phenotyping using massive feature extraction, *Cell Systems* **5**, 527 (2017).
- [63] B. D. Fulcher, Feature-based time-series analysis, in *Feature engineering for machine learning and data analytics* (CRC Press, 2018).
- [64] D.-P. Yang and P. A. Robinson, Critical dynamics of hopf bifurcations in the corticothalamic system: Transitions from normal arousal states to epileptic seizures, *Physical Review E* **95**, 10.1103/physreve.95.042410 (2017).
- [65] M. Ospeck, V. M. Eguíluz, and M. O. Magnasco, Evidence of a hopf bifurcation in frog hair cells, *Biophysical Journal* **80**, 2597 (2001).
- [66] D. O. Maoileidigh, E. M. Nicola, and A. J. Hudspeth, The diverse effects of mechanical loading on active hair bundles, *Proceedings of the National Academy of Sciences*, 1943 (2012).
- [67] J. E. Marsden, M. McCracken, J. E. Marsden, and M. McCracken, Examples, in *The Hopf Bifurcation and Its Applications* (Springer New York, New York, NY, 1976) pp. 136–150.
- [68] G. Deco, M. L. Kringelbach, V. K. Jirsa, and P. Ritter, The dynamics of resting fluctuations in the brain: Metastability and its dynamical cortical core, *Scientific Reports* **7**, 3095 (2017).
- [69] M. Schumaker, Center manifold reduction and normal form transformations in systems with additive noise, *Physics Letters A* **122**, 317 (1987).
- [70] J. Ferrell, Bistability, bifurcations, and waddington’s epigenetic landscape, *Current Biology* **22**, R458–R466 (2012).
- [71] P. E. Kloeden and E. Platen, *Numerical Solution of Stochastic Differential Equations* (Springer Berlin Heidelberg, 1992).
- [72] C. M. Thomas and J. A. Thomas, *Elements of Information Theory*, 2nd ed. (John Wiley & Sons, Nashville, TN, 2006).
- [73] S. R. Carpenter and W. A. Brock, Rising variance: a leading indicator of ecological transition, *Ecology Letters* **9**, 311 (2006).
- [74] Y.-C. Chen, A tutorial on kernel density estimation and recent advances, *Biostatistics & Epidemiology* **1**, 161 (2017), <https://doi.org/10.1080/24709360.2017.1396742>.
- [75] J. D. Hamilton, *Time Series Analysis* (Princeton University Press, 1994).
- [76] R. F. Bass, *Stochastic Processes*, Cambridge Series in Statistical and Probabilistic Mathematics (Cambridge University Press, Cambridge, 2011).
- [77] F. Takens, Detecting strange attractors in turbulence, in *Dynamical Systems and Turbulence, Warwick 1980: proceedings of a symposium held at the University of Warwick 1979/80* (Springer, 2006) pp. 366–381.
- [78] B. Harris, [brendanjoharris/criticality: v0.1.2](https://doi.org/10.1101/2023.01.12.524111) (2023).
- [79] D. Gunning, M. Stefik, J. Choi, T. Miller, S. Stumpf, and G.-Z. Yang, Xai—explainable artificial intelligence, *Science Robotics* **4**, 10.1126/scirobotics.aay7120 (2019).
- [80] P. Linardatos, V. Papastefanopoulos, and S. Kotsiantis, Explainable ai: A review of machine learning interpretability methods, *Entropy* **23**, 18 (2020).
- [81] A. Davies, P. Veličković, L. Buesing, S. Blackwell, D. Zheng, N. Tomašev, R. Tanburn, P. Battaglia, C. Blundell, A. Juhász, M. Lackenby, G. Williamson, D. Hassabis, and P. Kohli, Advancing mathematics by guiding human intuition with ai, *Nature* **600**, 70–74 (2021).
- [82] C. Tu, P. D’Odorico, and S. Suweis, Critical slowing down associated with critical transition and risk of collapse in crypto-currency, *Royal Society Open Science* **7**, 191450 (2022).
- [83] X.-Q. Xie, W.-P. He, B. Gu, Y. Mei, and J. Wang, The robustness of the skewness as an early warning signal for abrupt climate change, *International Journal of Climate*

- tology **39**, 5672 (2019).
- [84] V. Guttal and C. Jayaprakash, Changing skewness: an early warning signal of regime shifts in ecosystems, *Ecology Letters* , 450 (2008).
- [85] J. Lim and B. I. Epureanu, Forecasting a class of bifurcations: Theory and experiment, *Physical Review E* **83**, 016203 (2011).
- [86] T. Kaur and P. S. Dutta, Effects of noise correlation and imperfect data sampling on indicators of critical slowing down, *Theoretical Ecology* [10.1007/s12080-022-00532-2](https://doi.org/10.1007/s12080-022-00532-2) (2022).
- [87] B. Fulcher, O. Cliff, B. Harris, Philiphorst, S. Sethi, C. H. Lubba, I. Alam, lukas, K. P. Vysyaraju, J. McCormac, VP007-py, XavierFPMorris, and K. Shiina, [benfulcher/hctsa: v1.08](https://github.com/benfulcher/hctsa) (2023).